Inorganics **2015**, *3*, 82-100; doi:10.3390/inorganics3020082

OPEN ACCESS

inorganics

ISSN 2304-6740

www.mdpi.com/journal/inorganics

Communication

A Heteroaromatically Functionalized Hexamolybdate

Merinda R. Healey, Stephen P. Best, Lars Goerigk and Chris Ritchie *

School of Chemistry, University of Melbourne, Melbourne 3010, Australia;
E-Mails: healeym@student.unimelb.edu.au (M.R.H.); spbest@unimelb.edu.au (S.P.B.);
lars.goerigk@unimelb.edu.au (L.G.)

* Author to whom correspondence should be addressed; E-Mail: critchie@unimelb.edu.au;
Tel.: +61-390357419.

Academic Editors: Greta Ricarda Patzke and Pierre-Emmanuel Car

Received: 14 April 2015 / Accepted: 28 April 2015 / Published: 8 May 2015

Abstract: A new heteroaromatic thiophene containing organoimido functionalized hexamolybdate has been synthesized and characterized in both solid form and solution. Structural analysis shows successful introduction of the organoimido ligand through replacement of one terminal oxo site on $[Mo_6O_{19}]^{2-}$ to yield the singly functionalized hexamolybdate. Spectroscopic and theoretical analysis indicates charge transfer between the inorganic and organic components, with a significantly red-shifted lowest lying transition of 399 nm *vs.* the parent Lindqvist ion of 325 nm. Additional characterization includes, thermal gravimetric analysis (TGA), infrared (IR), cyclic voltammetry (CV), nuclear magnetic resonance (NMR) and time-dependent density functional theory (TD-DFT) studies.

Keywords: polyoxometalate; organoimido; dehydration; thiophene

1. Introduction

Recent interest in the development of methodologies for the covalent grafting of organic molecules to the surface of polyoxometalates (POMs) has been driven by the utility of the resulting inorganic-organic hybrids in a range of applications [1–6]. One such methodology can be used to yield organoimido functionalized Lindqvist structures of general formula $[Mo_6O_{(19-x)}(NR)_x]^{2-}$ where x = 1–6 and (NR) can be aromatic or aliphatic in nature [7]. Since the first report of organoimido

functionalized hexamolybdates, several groups have shown interest in the synthesis of this structural class, and have subsequently reported a variety of modified synthetic approaches and reaction conditions to achieve this goal [8–10]. That being said, drawing clear conclusions as to a rational synthetic approach from the literature is challenging when targeting multiple organoimido-substituted hexamolybdates. The use of aniline-based hydrochloride salts is a general synthetic route to the formation of mono-functionalized hexamolybdates and was first reported by Wei and Guo [11]. Both the aniline and its HCl salt were used for the synthesis of mono-functionalized complexes containing electron-withdrawing groups. This route involves the reaction of the α isomer of octamolybdate $[Mo_8O_{26}]^{4-}$ with the hydrochloride salt of the aromatic amine of choice in dry acetonitrile in the presence of the dehydrating and activating agent *N*,*N*'-Dicyclohexylcarbodiimide (DCC) [12].

Post-synthetic reactions involving organoimido hexamolybdates containing terminal halogen or ethynyl groups has now been well documented [9,13–17]. Both Sonogashira and Heck Pd-catalyzed carbon-carbon coupling reactions involving organoimido hexamolybdate complexes have been reported, showing their promise as building blocks in the design of elaborate molecular and polymeric compounds. Several key examples of post-synthetic Sonogashira and Heck couplings include the preparation of complexes bearing metal binding ligands [17] and the incorporation of the hexamolybdate in main chain polymers [16], as well as the preparation of polymers with POM containing pendant side chains [9]. From a synthetic standpoint it is significant to note the varying stabilities of $[Mo_6O_{(19-x)}(NR)_x]^{2-}$ complexes to the post-synthetic conditions used in these reactions, in particular the tolerance of the base. The complex reported herein is currently under investigation regarding its utility for inclusion in materials prepared using these methodologies.

2. Results and Discussion

Here, we report a novel mono-functionalized organoimido hexamolybdate $[Mo_6O_{18}(\mathbf{L4})]^{2-}$ (**1-L4**) where **L4** = 4-(4-bromo-5-methylthiophen-2-yl)-2,6-dimethylaniline. **L4** was synthesized via the palladium catalysed cross coupling of 3,5-dibromo-2-methylthiophene (**L1**) with {4-[(diphenylmethylidene)amino]-3,5-dimethylphenyl}boronic acid (**L2**) to yield *N*-[4-(4-bromo-5-methylthiophen-2-yl)-2,6-dimethylphenyl]-1,1-diphenylmethanimine (**L3**) that was then subsequently deprotected and used as the HCl salt, as shown in (Scheme 1). The synthesis of (**1-L4**) involved the preparation of a solution of $(Bu_4N)_4[Mo_8O_{26}]$ (0.0561 mmol) in dry acetonitrile (2 mL) to which 1.34 equivalents of 4-(4-bromo-5-methylthiophen-2-yl)-2,6-dimethylaniline and 2 equivalents of DCC were added. This solution was then sealed in a 5 mL biotage microwave vial and reacted at 120 °C for 90 min at 4 bar in a biotage initiator microwave reactor. On cooling to room temperature, the reaction mixture was filtered and the solvent removed under vacuum. The resulting oil was washed with diethyl ether and subsequently recrystallized from acetonitrile via diethyl ether vapor diffusion. Fractional crystallization was then required, with the yellow tetrabutylammonium (TBA) salt of $[Mo_6O_{19}]^{2-}$ crystalizing initially. The remaining solution was decanted, concentrated and subjected to further diethyl ether diffusion resulting in the desired compound, in moderate yield, over 5–10 days.

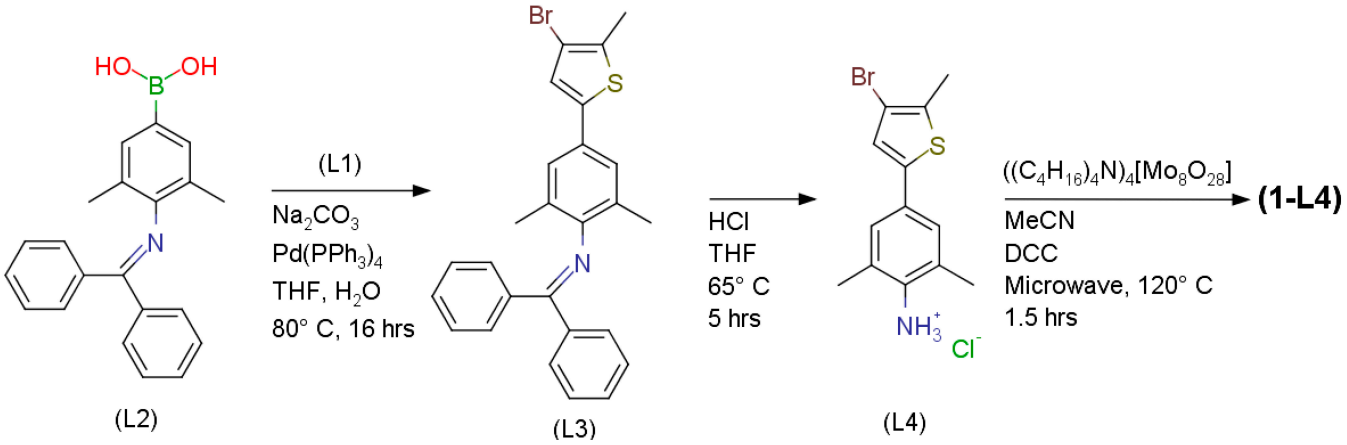

Scheme 1. Synthesis of the monofunctionalized organoimido hybrid (**1-L4**).

The molecular structure of (**1-L4**) (Figure 1) is characteristic of previously reported mono-imido hexamolybdates, with one of the terminal $[Mo{\equiv}O]^{4+}$ units being replaced by a more electron-rich $[Mo{\equiv}NR]^{4+}$ unit. The short Mo–N bond length (1.768(7) Å) and Mo–N–C bond angle (169.1(7)°) are in agreement with the assignment, and indicative of an Mo≡N triple bond character. Typical displacement of the central oxygen atom (O_c) within the hexamolybdate complex towards [O_c–Mo≡NR] (2.205(5) Å) *vs.* the average of the remaining non-substituted sites [O_c–Mo≡Ot] (2.34(1) Å) is also observed. Disorder of the thiophene portion of (**1-L4**) is observed due to free rotation around the single bond connecting the thiophene and aniline aromatic systems. The observed positions of carbon atoms C9, C12, and C13 were not affected by this disorder, whereas the positions of S1, C10, C11 the methyl substituent C14 and the bromine substituent Br1 were. Their positions were modeled using free variables, and by constraining the disordered atoms displacement parameters, atomic positions and bond lengths. The two observed positions refine well with occupancies of 58% and 42%. Furthermore, in the solid state the thiophene rings of two neighboring molecules are involved in pi-pi interactions resulting in the formation of a dimeric motif (Figure 1). The intermolecular separation was found to be 3.529(1) Å from ring center to ring center. Two charge balancing tetrabutyl-ammonium (TBA) cations are also required however only one could be successfully modeled, with the other showing significant disorder. A solvent mask was, therefore, implemented after the assignment of all locatable atoms from the difference map, with chemical and thermal analysis being consistent with the assignment of two TBA cations and the absence of any additional solvate in the bulk sample.

The electronic spectroscopy of (**1-L4**) (Figure A2) clearly shows a significant bathochromic shift and increase in intensity of the complexes lowest energy electronic absorption when compared to the parent plenary Linqvist polyanion $[Mo_6O_{19}]^{2-}$. Indeed this 72 nm shift to longer wavelengths (**1-L4** 399 nm *vs.* $[Mo_6O_{19}]^{2-}$ 325 nm) is among the largest observed for any mono-functionalized organoimido hexamolybdate with an $\varepsilon = 2.47 \times 10^4$ M^{-1} cm^{-1}. This absorption seems to be similar to other mono-functionalized compounds of extended conjugation presented in literature, such as that presented by Peng (382 nm, 392 nm, 403 nm) [15,17,18]. This significant bathochromic shift is indicative of extended conjugation between the organic and inorganic components, with the presence of the electron withdrawing –Br attached on the thiophene ring probably aiding electronic mobility within the hybrid material.

The nature of the absorption band for **1-L4** is further analyzed with linear-response time-dependent density functional theory (TD-DFT) calculations. Calculations at the TDA-CAMB3LYP/ def2-TZVPP [19–21] //TPSS-D3/def2-TZVP [21–24] level of theory show qualitative agreement with experiment with a bright transition at 390 nm. The blue-shift of 9 nm compared to the experimental value is within the usual error margin for this level of theory [25] and expected for gas-phase calculations. Further analysis reveals that this bright electronic excitation is dominated by a transition from the highest occupied (HOMO) to the lowest unoccupied molecular orbital (LUMO). The HOMO is predominantly localized around the imido bridge and the adjacent six-membered ring, while the LUMO is additionally characterized by a strong contribution from the thiophene unit (Figure A9a,b). Inspection of the difference density (Figure A9c) further confirms that this excitation is of charge-transfer (CT) character with the imido bridge functioning as the electron donor and the thiophene as the electron acceptor; see also References [26] and [27] for related computational work.

The initial voltammetric response from solutions of (**1-L4**) reveal a reversible reduction with $E^{\circ\prime} = -1.07$ V with an additional weak, reversible process with $E^{\circ\prime} = -0.92$ V, due to contamination of the sample by $[Mo_6O_{19}]^{2-}$ (Figure 2). The presence of $[Mo_6O_{19}]^{2-}$ in the sample allows quantification of the shift in reduction potential with functionalization of the plenary Lindqvist polyanion. A scan to strongly reduce potentials lower than −1.65 V is accompanied by formation of daughter products which give rise to distinct anodic processes at potentials above 0.1 V (Figure A8), which are due to decomposition products. Similar anodic waves have previously been attributed to the oxidation of isopoly blues of unknown composition [28]. Consistent with earlier reports, there is evidence for surface adsorption of the reduced polyoxo species with subsequent voltammograms featuring increasingly current with broad and sharp features consistent with a mixture of surface immobilized and solute species.

FTIR spectroscopy of (**1-L4**) (Figure A4) shows the presence of several bands associated with the polyanion such as ν(Mo-O_t) and ν(Mo-O_b-Mo) stretches at 950 and 794 cm^{-1}, respectively. The characteristic ν(Mo-N) is observed as a sharp shoulder band at 975 cm^{-1}.

The solution stability of (**1-L4**) has been confirmed by ^1H NMR studies (Figure A7), with all protons being unambiguously assigned *versus* that observed for the (**L4**) starting material. Aryl aniline protons give a singlet at 7.30 ppm 2H, meanwhile the thiophene proton also gives a singlet at 7.23 ppm 1H. These peaks integrate well with the two sets of aniline methyl protons 2.62 ppm 6H and thiophene methyl protons 2.43 ppm 3H. Signals at 0.97, 1.35, 1.60, and 3.08 ppm are attributed to the protons in the tetrabutylammonium counterions. Higher integrations of the cation protons indicate the possibility of some residual hexamolybdate that could not be separated via fractional crystallization or during the isolation process. (**1-L4**) was also studied by LC-MS showing isotopic cluster anions centered at *m*/*z* 579.16, and 1159.39. The signals are thus assigned as the parent cluster M^{2-} (M = $[Mo_6O_{18}NC_{13}SH_{12}Br]$), calculated 579.17 and $M^{2-} + H^+$, calculated 1159.38 (Figure A1).

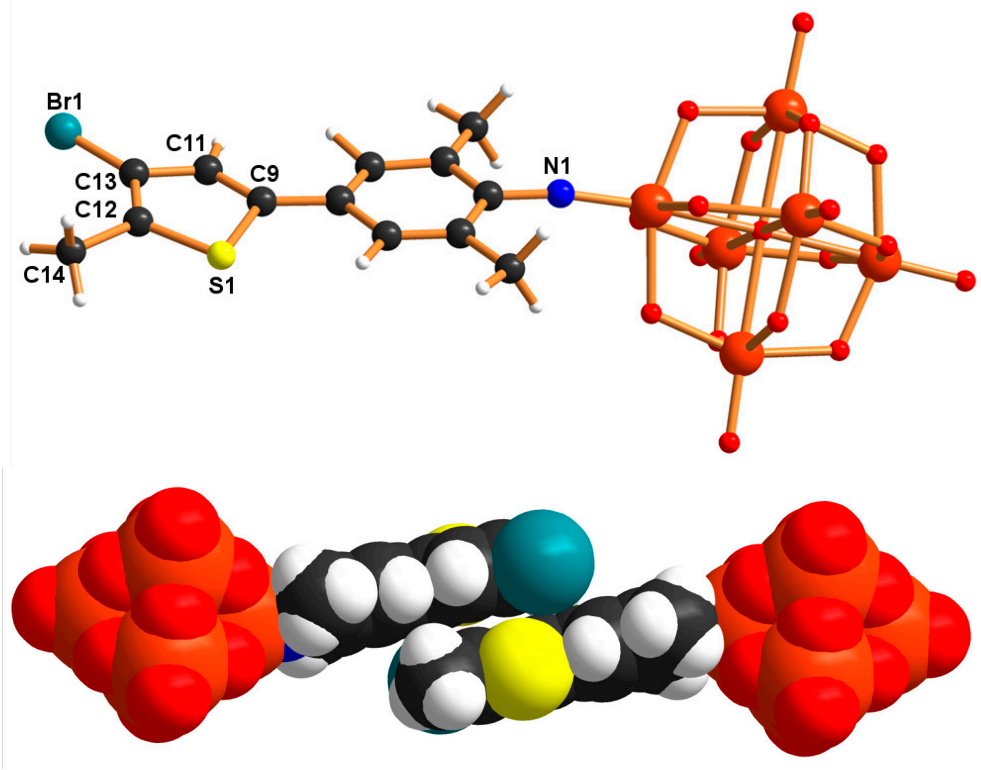

Figure 1. Graphical representation of (**1-L4**) (**top**) and space filling representation of the pi-stacked dimers observed in the solid state (**bottom**). Mo = Orange spheres; O = Red spheres; N = Blue sphere, C = Black spheres; S = Yellow sphere; Br = Teal sphere; H = White spheres [29].

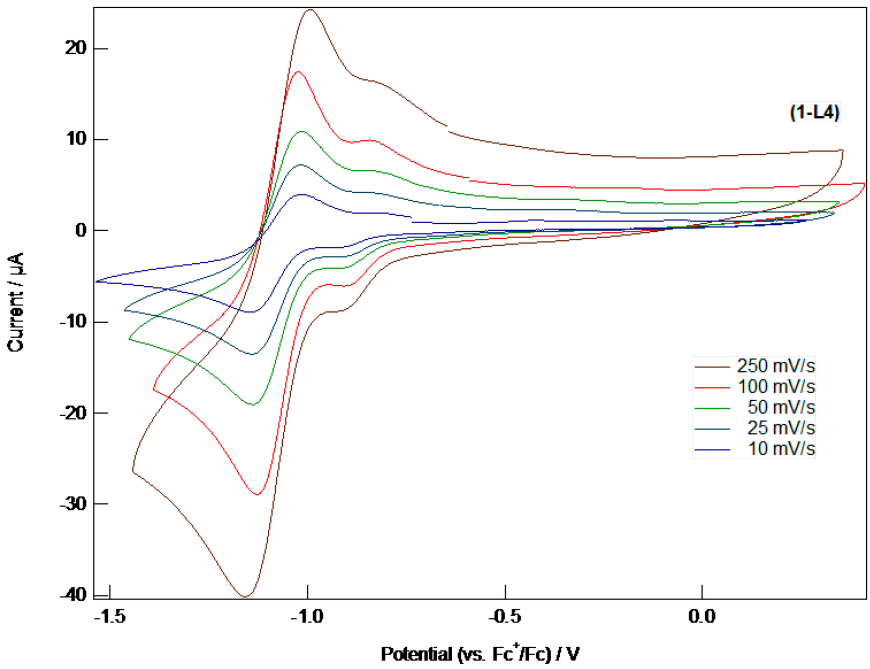

Figure 2. Cyclic voltammetry of a 2 mM solution of (**1-L4**) with $(Bu_4N)PF_6$ (0.1 M) in CH_3CN. The scans were recorded from a freshly polished electrode using Pt working (3 mm diameter) and counter electrodes and an Ag pseudo-reference electrode. Potentials were corrected *vs.* ferrocene.

3. Conclusions

A new heteroaromatically derivatized hexamolybdate has been synthesized and extensively characterized. Theoretical TD-DFT calculations qualitatively agree with experimental observations, with the lowest lying excitation having charge transfer character whereby the HOMO is localized around the organoimido bridge and the LUMO on the thiophene. The electrochemical response of (**1-L4**) is similar to that of the parent Lindqvist polyanion with the potential of the first reversible reduction shifted cathodically by 150 mV as a result of derivitization. The reversibility of the process indicates that the reduced compound does not undergo dissociation of the ligand or fragmentation over the timeframe of the cyclic voltammetric experiment. Further reduction results in rapid decomposition of the complex. The molecule represents a rare example of a halogenated organoimido functionalized hexamolybdate with potential for further post-synthetic modification as a result, which is currently under investigation.

Acknowledgments

CR and LG are recipients of Australian Research Council Discovery Early Career Researcher Awards (project numbers DE130100615 and DE140100550) LG also acknowledges funding from the Selby Scientific Foundation through the 2014 Selby Research Award and generous allocation of computing time from the National Computational Infrastructure (NCI) National Facility within the National Computational Merits Allocation Scheme (project fk5). MRH acknowledges funding from the Australian Government and the University of Melbourne in the form of an Australian Postgraduate Award (APA).

Author Contributions

CR conceived the work, with the synthetic work, crystallization and characterization completed by MRH. The X-ray data was collected by MRH and the structure solved and refined with the assistance of CR. SPB, with assistance of MRH conducted the electrochemistry and LG conducted the TD-DFT calculations. The manuscript was written with contributions from all authors.

Appendix

IR, ^{1}H NMR spectra, TGA and X-ray data collection and refinement details of **L3, L4** and **1-L4** are available where applicable. Crystal structures of (**1-L4**) and (**L3**) are deposited in the Cambridge Structural Database as CCDC 1057033 and 1057032.

A1. Instrumentation

A1.1. FT-IR Spectroscopy (KBr Disc)

FT-IR spectroscopy was performed on a Bruker Tensor 27 FT-IR spectrometer (University of Melbourne, Melbourne, Australia). Samples were prepared as KBr pellets. Signals are listed as wavenumbers (cm^{-1}) with the following abbreviations: vs = very strong, s = strong, m = medium, w = weak and b = broad.

A1.2. Elemental Analysis

Chemical analysis was performed on Carlo Erba Elemental Analyser EA 1108, (The Campbell Microanalytical Laboratory, Department of Chemistry, University of Otago, Otago, New Zealand).

A1.3. Microwave Reactor

Synthesis of (**1-L4**) was performed using a Biotage Initiator (University of Melbourne, Melbourne, Australia).

A1.4. UV-Vis Spectrometer

UV-Vis spectroscopy was performed on Agilent Technologies Cary 60 UV-Vis (University of Melbourne, Melbourne, Australia), using standard quartz cuvettes (d = 1 cm).

A1.5. Mass Spectroscopy (ESI)

Mass spectroscopy was performed on a high resolution Agilent QTOF LCMS 6520 (University of Melbourne, Melbourne, Australia).

A1.6. Thermogravimetric Analysis (TGA)

Thermal analysis was performed on a Mettler TGA/SDTA851^e Module (University of Melbourne, Melbourne, Australia). Method: gas flow: N_2 at 25 mL/min, temperature: 25 °C (5 min), 25–450 °C (rate: 5 °C/min)

A1.7. NMR Spectroscopy

NMR spectroscopy was performed on a Varian 400 MHz NMR Spectrometer (University of Melbourne, Melbourne, Australia).

A1.8. Column Chromatography

Chromatographic separations were performed using a Grace Technologies, Reveleris X2 (University of Melbourne, Melbourne, Australia).

A1.9. Electrochemistry

Electrochemical experiments were conducted using a purpose built cell previously described [30]. Experiments employed 3 mm diameter platinum working, silver pseudo-reference and platinum foil counter electrodes. Solutions for electrochemical analysis were prepared under strictly anaerobic conditions using a Vacuum Atmospheres glove box. The applied potential was controlled using a PAR model 362 potentiostat where waveforms were generated using EChem V1.5.2 software in conjunction with a Powerlab 4/20 interface (ADInstruments, University of Melbourne, Melbourne, Australia).

A2. Experimental Section

Chemicals were used as purchased without further purification. Solvents were degassed and dried over 3 Å molecular sieves using standard laboratory procedures. Previously reported compounds (**L1**) and (**L2**) were synthesised as described in the original paper [31].

Synthesis of (L3): *N*-[4-(4-bromo-5-methylthiophen-2-yl)-2,6-dimethylphenyl]-1,1-diphenylmethanimine

To a solution of *N*-(4-borate-2,6-dimethylphenyl)-1,1-diphenylmethanimine (820 mg, 2.25 mmol), Na_2CO_3 (360 mg, 3.40 mmol) and 3,5-dibromo-2-methylthiophene (563 mg, 2.25 mmol) in degassed THF (5 mL) and degassed water (3 mL), was added $Pd(PPh_3)_4$ (26 mg, 0.02 mmol) and the solution was purged with N_2 for 5 min. The reaction vessel was then sealed and heated to 80 °C for 16 h. Upon cooling, saturated aqueous NH_4Cl was added and the solution extracted with diethyl ether and dried with magnesium sulphate. The solution was then dried in vacuo and purified using column chromatography (silica, hexane : ethyl acetate, 0–5% ethyl acetate gradient flow over 10 min, R_f – 0.41 5% Ethyl acetate in hexane), to give a yellow solid. (1.036 g, 0.827 mmol, 37% yield). Recrystallization from acetone afforded large yellow blocks after 2 days via slow evaporation. ^{1}H NMR ($CDCl_3$, 400 MHz): δ 2.06 (s, 6H, Ar–CH_3), 2.38 (s, 3H, Ar–CH_3), 6.97 (s, 1H, ArH), 7.06 (s, 2H, ArH), 7.12(t, 2H, ArH), 7.23(t, 2H, ArH), 7.29 (t, 1H, ArH), 7.43 (t, 2H, ArH), 7.50 (t, 1H, ArH), 7.79 (d, 2H, ArH). Elemental analysis (%) calcd. For $C_{26}H_{22}NSBr$: C, 67.81; H, 4.82; N, 3.04. Found: C, 68.05; H, 4.96; N, 3.01. Selected IR data (KBr, cm^{-1}): 3053 (m), 3026 (w), 2966 (m), 2912 (m), 2853 (w), 1620 (vs), 1597 (s), 1576 (m), 1539 (m), 1490 (s), 1462 (s), 1445 (vs), 1377(w), 1329 (w), 1313 (s), 1286 (s), 1227 (s), 1180 (m), 1163 (m), 1137 (s), 1059 (s), 1028 (m), 999 (m), 976 (w), 949 (s), 912 (m), 885 (m), 864 (m), 849 (m), 820 (vs), 785 (s), 771 (s), 760 (m), 746 (m), 700 (vs), 648 (s), 617 (w), 590 (m), 557 (m), 505 (m).

Synthesis of (L4): (4-bromo-5-methylthiophen-2-yl)-2,6-dimethylaniline·HCl

To a solution of *N*-[4-(4-bromo-5-methylthiophen-2-yl)-2,6-dimethylphenyl]-1,1-diphenylmethanimine (1.00 g, 2.17 mmol) in THF (20 mL) was added HCl (2M, 10 mL) and heated at 65 °C for 5 h. The solution was then cooled, dried in vacuo and washed with ether to give an off white product (642.8 mg, 1.93 mmol, 89% yield). ^{1}H NMR (d6-DMSO, 400 MHz): δ 2.19 (s, 6H, Ar–CH_3), 2.34 (s, 3H, Ar–CH_3), 7.19 (s, 2H, ArH), 7.21 (s, 1H, ArH). Elemental analysis (%) calcd. For $C_{13}H_{15}NSClBr$: C, 46.93; H, 4.55; N, 4.21. Found: C, 46.37; H, 4.48; N, 4.19. Selected IR data (KBr, cm^{-1}): 3058(w), 2922 (w), 2852 (w), 2581 (w), 1621 (s), 1521(w), 1494 (m), 1468 (w), 1384 (m), 1318 (m), 1099 (w), 1063 (w), 818 (w), 786 (m).

Synthesis of (1-L4): Mo_6O_{18}(4-(4-bromo-5-methylthiophen-2-yl)-2,6-dimethylaniline)

A solution of $(Bu_4N)_4[Mo_8O_{26}]$ (120.8 mg, 0.0561 mmol), dicyclohexylcarbodiimide (23.1 mg, 0.112 mmol), 4-(4-bromo-5-methylthiophen-2-yl)-2,6-dimethylaniline.HCl (25 mg, 0.0751 mmol) in dry acetonitrile was heated in a microwave reactor at 120 °C for 90 min. The solution was then cooled, filtered and the remaining solvent removed in vacuo. The oil was then washed with diethyl ether and

dissolved in acetonitrile with vapor diffusion of diethyl ether resulting in the crystallization of hexamolybdate, which was removed by filtration. Further diffusion resulted in the crystallization of the desired red product (12 mg, 0.00730 mmol, 13% yield) after one week. ^{1}H NMR (CD_3CN, 400 MHz): δ 0.97 (t, 24H, $–CH_3$, $[Bu_4N]^+$), 1.35 (m, 16H, $–CH_2–$, $[Bu_4N]^+$), 1.60 (m, 16 H, $–CH_2–$, $[Bu_4N]^+$), 2.43 (s, 3H, $Ar–CH_3$), 2.62 (s, 6H, $Ar–CH_3$), 3.08 (m, 16H, $–CH_2–$, $[Bu_4N]^+$), 7.23 (s, 1H, ArH), 7.30 (s, 2H, ArH). Elemental analysis (%) calcd. For $C_{45}H_{84}N_3SBrMo_6O_{18}$: C, 32.90; H, 5.16; N, 2.56. Found: C, 32.98; H, 5.25; N, 2.53. Selected IR data (KBr, cm^{-1}): 2961(s), 2932 (w), 2873 (m), 1626 (m), 1595 (w), 1479 (m), 1382 (m), 1320 (m), 1161 (w), 975 (s, Mo–N), 950 (vs, $Mo–O_t$), 880 (w), 794 (vs, Mo–O–Mo), 590 (m), 448 (m).

A3. Characterization Section

A3.1. Mass Spectroscopy

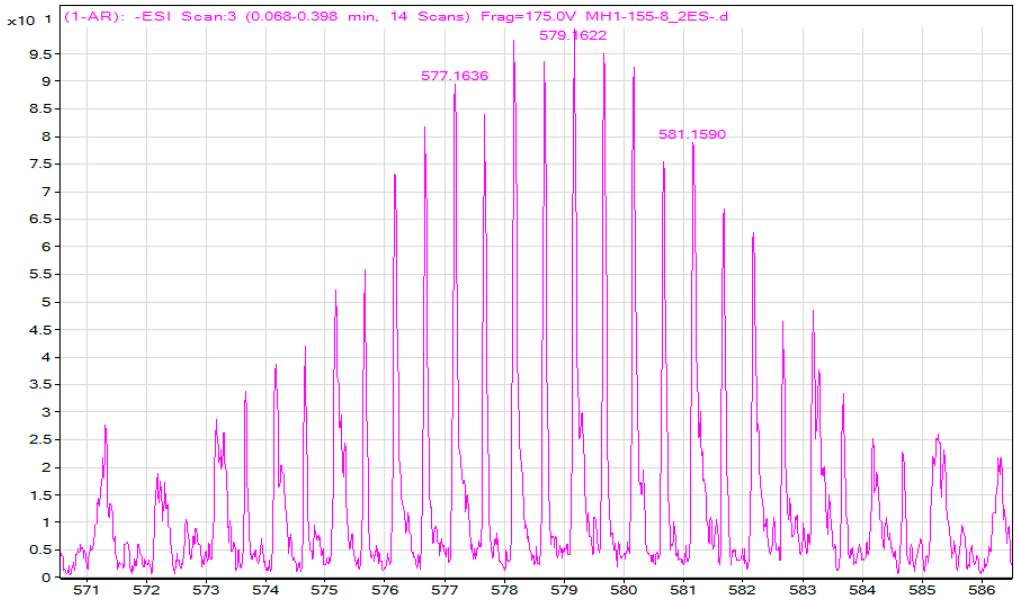

Figure A1. Mass Spectrum of Compound (**1-L4**) ($M^{2–}$, *m*/*z* = 579.16). ESI mass spectrometry was performed in acetonitrile in negative ion mode.

A3.2. Electronic Spectroscopy

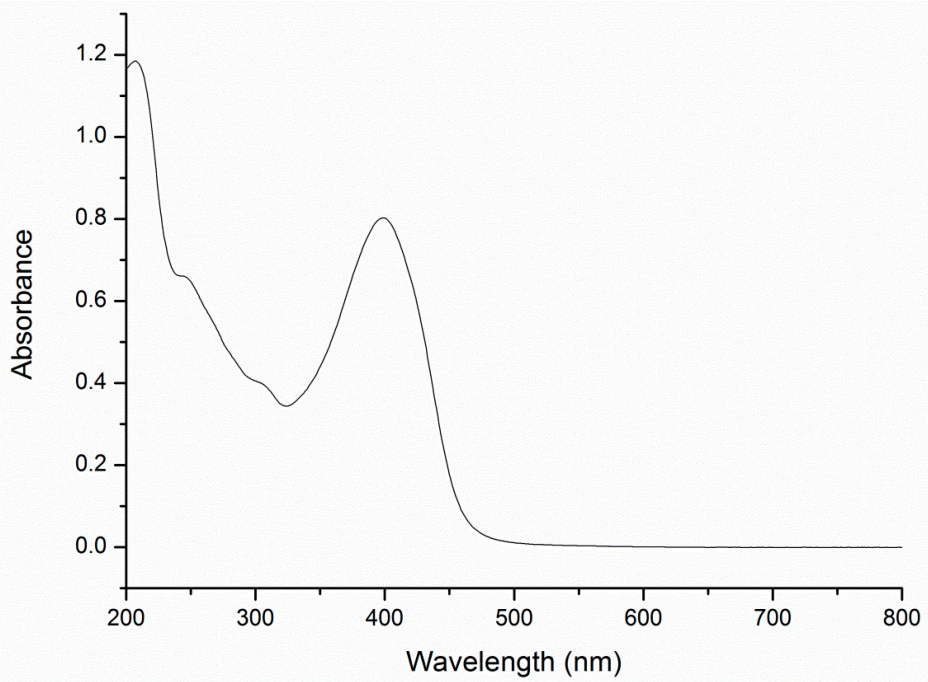

Figure A2. UV-Vis spectrum of (**1-L4**) in MeCN: λ_{max1} = 399 nm, ε = 2.47 × 10^4 M^{-1} cm^{-1}, λ_{max1} = 305 nm, ε = 1.23 × 10^4 M^{-1} cm^{-1}, λ_{max1} = 246 nm, ε = 2.03 × 10^4 M^{-1} cm^{-1}1, λ_{max1} = 207 nm, ε = 3.65 × 10^4 M^{-1} cm^{-1}.

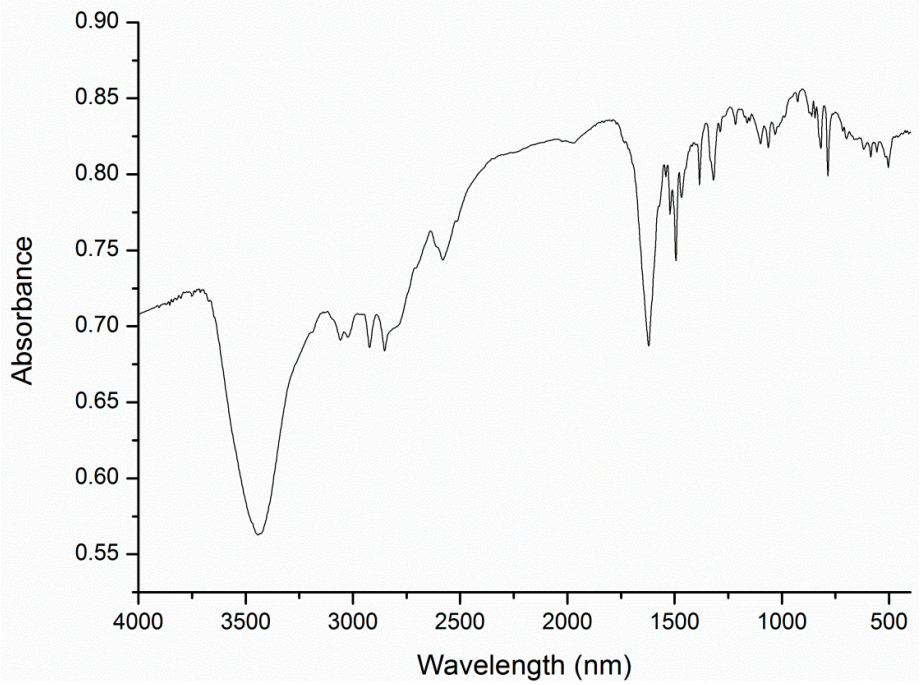

Figure A3. IR spectrum of (**L4**).

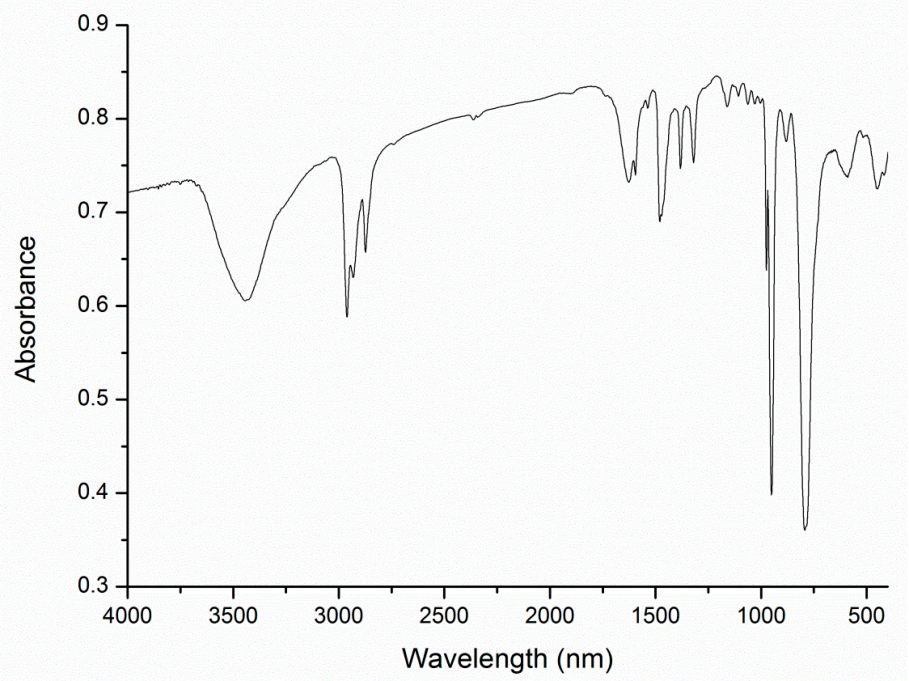

Figure A4. IR spectrum of (**1-L4**).

A3.3. Nuclear Magnetic Resonance Spectroscopy

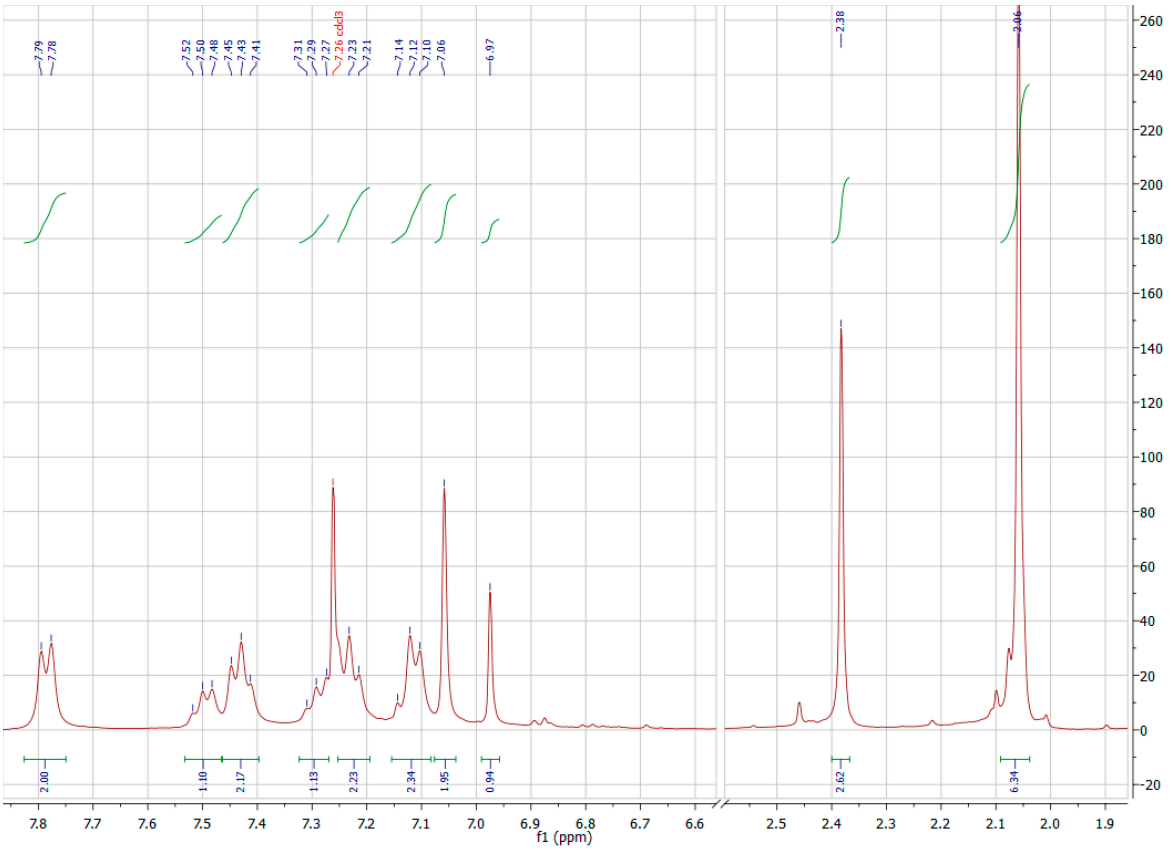

Figure A5. NMR Spectrum (400 MHz) of (**L3**) in $CDCl_3$.

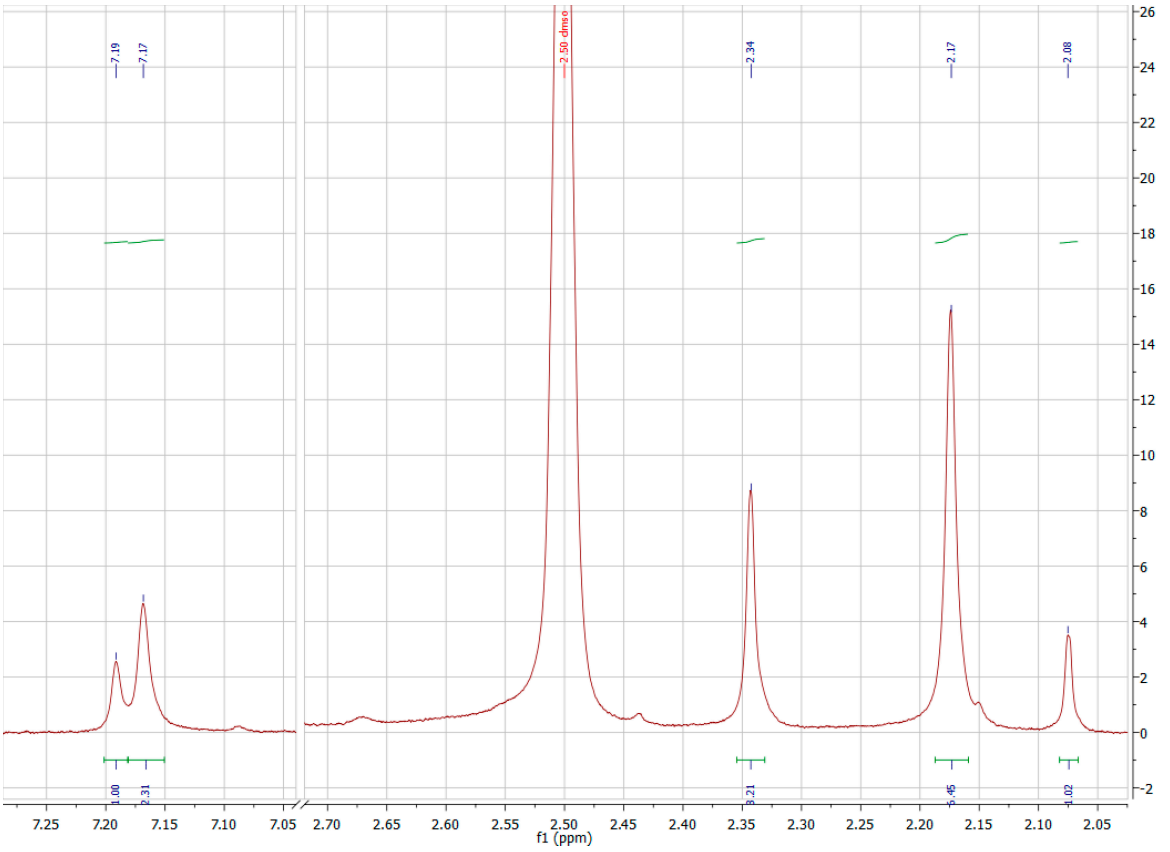

Figure A6. NMR Spectrum (400 MHz) of (**L4**) in d6-DMSO.

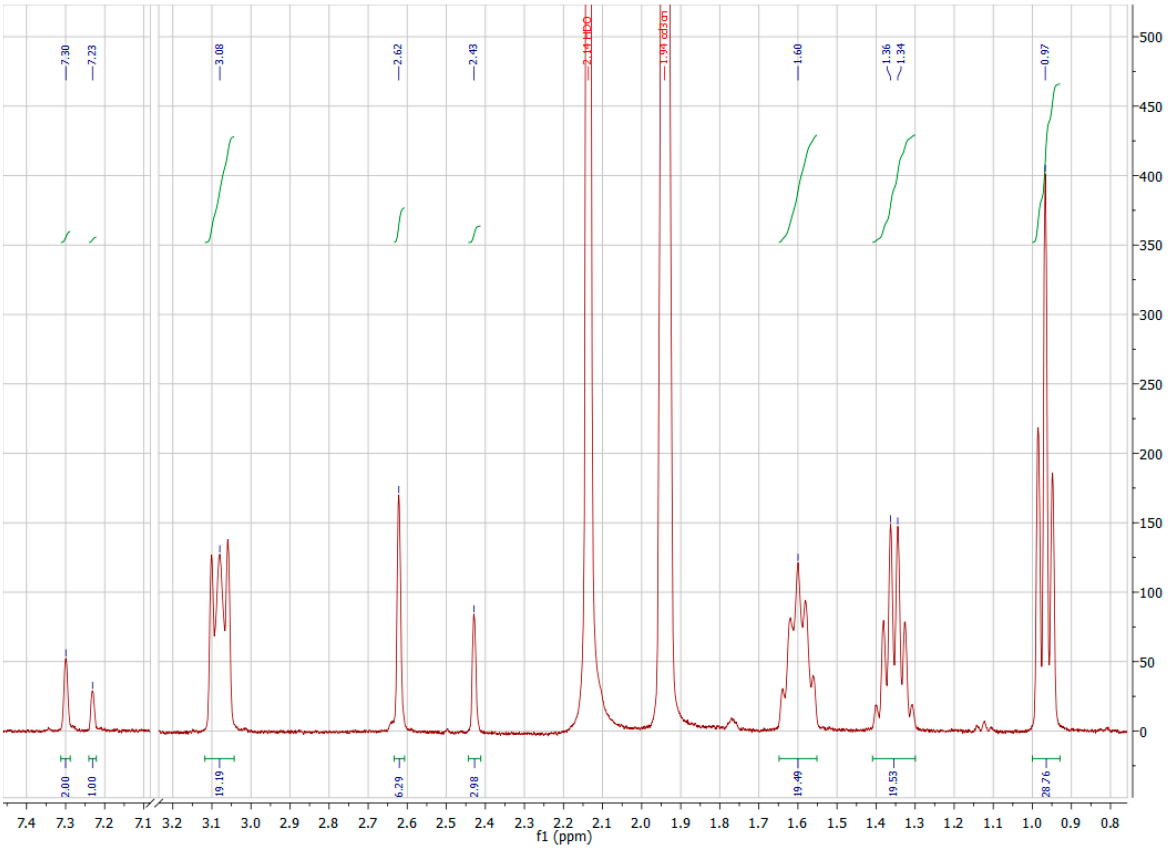

Figure A7. NMR Spectrum (400 MHz) of (**1-L4**) in d3-MeCN.

A3.4. Electrochemistry

Following the completion of voltammetric experiments a sample of ferrocene (Fc) was added to the solution and all potentials are referenced against the Fc^+/Fc couple.

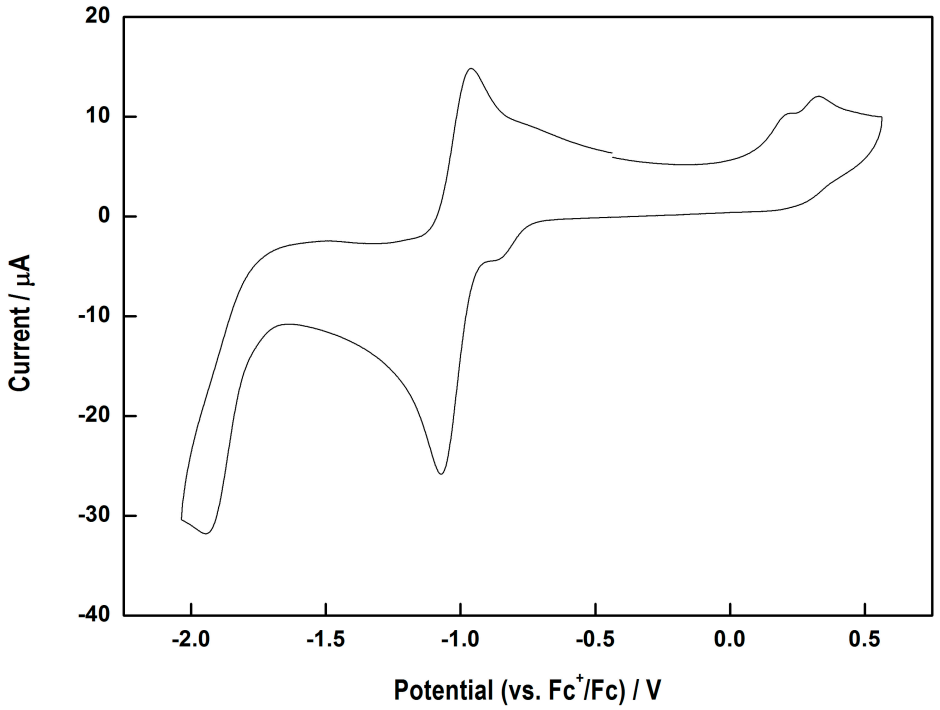

Figure A8. Cyclic voltammetry of (**1-L4**) showing the second reduction and accompanying anodic processes.

A3.5. Computational Details

The geometry optimization of one (**1-L4**) unit was carried out with TURBMOLE 6.4 [32], the TPSS [22] meta-generalized-gradient-approximation density functional, and Ahlrichs' triple-ζ atomic-orbital (AO) basis set with one set of polarization functions (def2-TZVP) [21]. The modified Stuttgart-Dresden def2-ECP [21] effective core potential was applied to the Mo atoms. Grimme's DFT-D3 [23] London-dispersion correction with Becke-Johnson damping [24] was applied during this step. Subsequent linear-response time-dependent density functional theory calculations were carried out with ORCA 3.0.2 [33] within the Tamm-Dancoff approximation (TDA) [19]. For all heavy atoms, the def2-TZVPP AO basis set was applied, while hydrogen atoms were treated with the def2-SV double-ζ basis to speed up the calculations [21]. The def2-ECP was again applied to all Mo atoms.

The results discussed in the manuscript were obtained with the range-separated CAMB3LYP density functional [20]. Additional calculations with the range-separated wB97X-D3 [34] functional confirmed the charge-transfer character of the first bright excitation and were in qualitative agreement with the CAMB3LYP calculations (absorption at 379 nm). The resulting highest occupied and lowest unoccupied molecular orbitals obtained at the CAMB3LYP level are shown in Figure A9, along with the difference density, and they clearly indicate the charge-transfer character of the excitation.

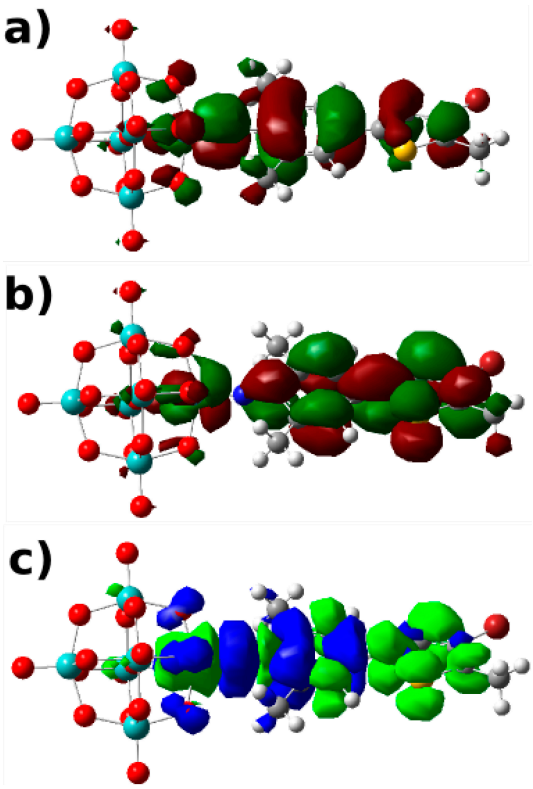

Figure A9. (**a**) Highest occupied molecular orbital obtained at the CAMB3LYP/def2-TZVPP level of theory displayed with an isovalue of 0.02 $e^{-}/Å^{33}$. (**b**) Lowest unoccupied molecular orbital obtained at the CAMB3LYP/def2-TZVPP level of theory displayed with an isovalue of 0.02 $e^{-}/Å^{33}$. (**c**) Difference density for the CT transition obtained at the TDA-CAMB3LYP/def2-TZVPP level of theory displayed with an isovalue of 0.0004 $e^{-}/Å^{33}$. Green lobes indicate an increase in electron density upon electronic excitation and blue indicates a decrease. All surface plots were generated with Gaussview 5.0 [34].

A3.6. Cartesian Coordinates

Table A1. Cartesian Coordinates (Å) of 1-L4 Optimized at the TPSS-D3/def2-TZVP Level of Theory.

	Cartesian Coordinates (Å)		
H	3.76704225	2.03847542	0.30065425
C	8.79961983	−2.01560166	0.41244729
H	8.87077619	−2.73103735	−0.41655383
H	9.69833234	−1.39231526	0.40394112
H	8.78913391	−2.59102756	1.34634501
C	0.96256278	0.13987740	−0.04620859
C	1.56254262	−1.14797725	−0.14917984
C	1.77530740	1.29901199	0.10936217
C	2.94484244	−1.24373548	−0.09804489
H	3.40180409	−2.22830515	−0.19445924
C	1.10163712	2.63869224	0.22587839
H	0.50481002	2.85061645	−0.66856868
H	1.83866424	3.43685064	0.36309774

Table A1. *Cont.*

Cartesian Coordinates (Å)			
H	0.39680786	2.64829174	1.06459060
C	7.59386438	−1.14230232	0.28740460
C	6.18839822	0.74582657	0.03186394
H	5.97589682	1.79675983	−0.11316036
C	3.15321125	1.15160124	0.15798309
C	3.77009862	−0.11209650	0.05490087
C	0.67156702	−2.34846316	−0.30992473
H	−0.01800377	−2.43524581	0.53732293
H	1.26335447	−3.26621562	−0.38903123
H	0.03677621	−2.24804774	−1.19713465
C	5.21655957	−0.23465473	0.11026329
C	7.50055059	0.21728381	0.13429621
N	−0.37806453	0.25874441	−0.08920770
O	−6.30236442	1.57923483	−1.41436027
O	−4.37228812	0.26702048	−0.09343012
O	−2.55751051	1.59712153	−1.44792530
O	−6.29892939	1.59573674	1.21226320
O	−4.41902666	2.91549342	−0.08453437
O	−2.55711831	1.61203372	1.24718283
O	−4.42922706	0.27669877	−2.74280726
O	−6.29344006	−1.04499882	1.23892385
O	−4.43233273	0.25667581	2.55667783
O	−6.29498094	−1.05586386	−1.40947046
O	−2.55700529	−1.08720380	−1.42217494
O	−4.46304402	3.15757998	−2.93033868
O	−2.55518400	−1.06732613	1.24923151
O	−4.45481996	3.10375150	2.79799406
O	−8.47713797	0.24262438	−0.08541032
O	−4.44104229	−2.38607044	−0.10306189
O	−4.42260783	−2.62719372	2.74380416
O	−4.43177656	−2.57234737	−2.98509932
S	5.98186692	−1.79775572	0.31727666
BR	9.04012899	1.35225338	0.04645216
MO	−4.45217513	1.95216728	−1.72269566
MO	−6.77320756	0.24249817	−0.08640557
MO	−4.44116305	1.89427511	1.59437427
MO	−2.16185379	0.29537333	−0.10077312
MO	−4.40705584	−1.42246356	1.53532479
MO	−4.41479636	−1.36432115	−1.77989579

A3.7. Crystallography

Table A2. X-ray Data Collection. Single crystal X-ray data was collected using an Agilent Technologies SuperNova Dual Wavelength single crystal X-ray diffractometer at 130 K using Mo-Kα radiation (λ = 0.71073 Å) for (**L3**) and Cu-Kα radiation (λ = 1.5418 Å) for (**1-L4**) fitted with a mirror monochromator. Crystals were transferred directly from the mother liquor to the oil, to prevent solvent loss. The data was reduced using CrysAlisPro software (Version 1.171.36.28) (University of Melbourne, Melbourne, Australia) using a numerical absorption correction based on Gaussian integration over a multifaceted crystal model. Data was solved using direct methods by SHELXT and refined using a full-matrix least square procedure based upon F^2. All ordered non-H atoms were refined anisotropically.

Parameter	**L3**	**1-L4**
Formula	$C_{26}H_{22}NSBr$	$Mo_6O_{18}N_3C_{45}H_{84}SBr$
F_w	460.41	1642.76
Crystal Class	Monoclinic	Monoclinic
Space Group	$P2_1/n$	$P2_1/n$
a (Å)	12.5989(5)	11.03023(16)
b (Å)	11.5694(5)	16.9232(2)
c (Å)	15.2670(6)	32.4507(5)
α (°)	90	90
β (°)	101.954(4)	98.8238(13)
γ (°)	90	90
V (Å^3)	2177.07(16)	5985.79(15)
Z	4	4
T (K)	130.01(10)	130.01(10)
μ (mm^{-1})	1.996	11.658
reflns measd	13729	105913
unique reflns	5687	12538
R1 [$I > 2\sigma(I)$]	0.0497	0.0898
*w*R2(all data)	0.1727	0.2471

A3.8. Thermal Gravimetric Analysis

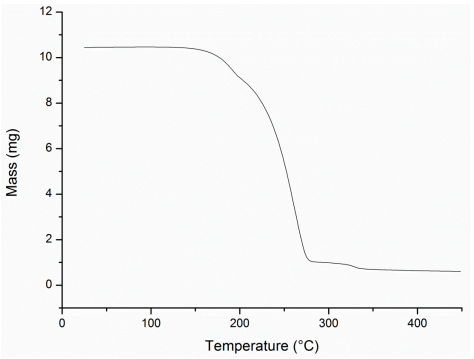

Figure A10. TGA of Compound (**L4**), showing that no solvent is present within the structure, which is in line with the elemental analysis.

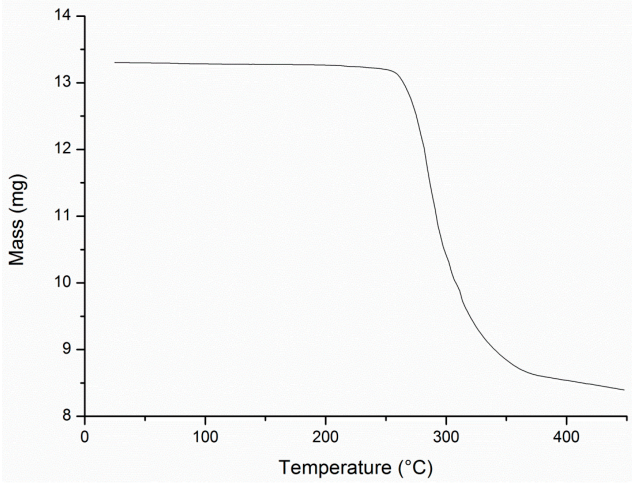

Figure A11. TGA of Compound (**1-L4**), showing that no solvent is present within the structure, which is in line with the crystal structure and elemental analysis.

Conflicts of Interest

The authors declare no conflict of interest.

References

1. An, H.Y.; Wang, E.B.; Xiao, D.R.; Li, Y.G.; Su, Z.M.; Xu, L. Chiral 3D architectures with helical channels constructed from polyoxometalate clusters and copper-amino acid complexes. *Angew. Chem. Int. Ed. Engl.* **2006**, *45*, 904–908.
2. Zhang, J.; Song, Y.; Cronin, L.; Liu, T. Self-assembly of organic-inorganic hybrid amphiphilic surfactants with large polyoxometalates as polar head groups. *J. Am. Chem. Soc.* **2008**, *130*, 14408–14409.
3. Song, Y.F.; McMillan, N.; Long, D.L.; Thiel, J.; Ding, Y.; Chen, H.; Gadegaard, N.; Cronin, L. Design of hydrophobic polyoxometalate hybrid assemblies beyond surfactant encapsulation. *Chemistry* **2008**, *14*, 2349–2354.
4. Song, Y.; McMillan, N.; Long, D.; Kane, S.; Malm, J.; Riehle, M.O.; Pradeep, C. P.; Gadegaard, N.; Cronin, L. Micropatterned surfaces with covalently grafted unsymmetrical polyoxometalate-hybrid clusters lead to selective cell adhesion. *J. Am. Chem. Soc.* **2009**, *131*, 1340–1341.
5. Aronica, C.; Chastanet, G.; Zueva, E.; Borshch, S.A.; Clemente-Juan, J.M.; Luneau, D. A mixed-valence polyoxovanadate(III,IV) cluster with a calixarene cap exhibiting ferromagnetic V(III)-V(IV) interactions. *J. Am. Chem. Soc.* **2008**, *130*, 2365–2371.
6. Pan, D.; Chen, J.; Tao, W.; Nie, L.; Yao, S. Polyoxometalate-modified carbon nanotubes: New catalyst support for methanol electro-oxidation. *Langmuir* **2006**, *22*, 5872–5876.
7. Strong, J.B.; Yap, G.P.A.; Ostrander, R.; Liable-Sands, L.M.; Rheingold, A.L.; Thouvenot, R.; Gouzerh, P.; Maatta, E.A. A New Class of Functionalized Polyoxometalates: Synthetic, Structural, Spectroscopic, and Electrochemical Studies of Organoimido Derivatives of $[Mo_6O_{19}]^{2-}$. *J. Am. Chem. Soc.* **2000**, *122*, 639–649.

8. Proust, A.; Thouvenot, R.; Chaussade, M.; Robert, F.; Gouzerh, P. Phenylimido derivatives of $[Mo_6O_{19}]^{2-}$: Syntheses, X-ray structures, vibrational, electrochemical, ^{95}Mo and ^{14}N NMR studies. *Inorg. Chim. Acta* **1994**, *224*, 81–95.
9. Moore, A.R.; Kwen, H.; Beatty, A.M.; Maatta, E.A. Organoimido-polyoxometalates as polymer pendants. *Chem. Commun.* **2000**, *996*, 1793–1794.
10. Wei, Y.; Xu, B.; Barnes, C.L.; Peng, Z. An Efficient and Convenient Reaction Protocol to Organoimido Derivatives of Polyoxometalates. *J. Am. Chem. Soc.* **2001**, *123*, 4083–4084.
11. Wu, P.; Li, Q.; Ge, N.; Wei, Y.; Wang, Y.; Wang, P.; Guo, H. An Easy Route to Monofunctionalized Organoimido Derivatives of the Lindqvist Hexamolybdate. *Eur. J. Inorg. Chem.* **2004**, *2004*, 2819–2822.
12. Li, Q.; Wu, P.; Xia, Y.; Wei, Y.; Guo, H. Synthesis, spectroscopic studies and crystal structure of a polyoxoanion cluster incorporating para-bromophenylimido ligand, $(Bu_4N)_2[Mo_6O_{18}(NC_6H_4Br\text{-}p)]$. *J. Organomet. Chem.* **2006**, *691*, 1223–1228.
13. Xu, B.; Wei, Y.; Barnes, C.L. Hybrid Molecular Materials Based on and Organic Conjugated Systems. *Angew. Chem. Int. Ed. Engl.* **2001**, *40*, 2290–2292.
14. Lu, M.; Wei, Y.; Xu, B.; Cheung, C.F.C.; Peng, Z.; Powell, D.R. Hybrid molecular dumbbells: bridging polyoxometalate clusters with an organic pi-conjugated rod. *Angew. Chem. Int. Ed. Engl.* **2002**, *41*, 1566–1568.
15. Kang, J.; Nelson, J.A.; Lu, M.; Xie, B.; Peng, Z.; Powell, D.R. Charge-transfer hybrids containing covalently bonded polyoxometalates and ferrocenyl units. *Inorg. Chem.* **2004**, *43*, 6408–6413.
16. Lu, M.; Xie, B.; Kang, J.; Chen, F.; Peng, Z. Synthesis of Main-Chain Polyoxometalate-Containing Hybrid Polymers and Their Applications in Photovoltaic Cells. *Chem. Mater.* **2005**, *17*, 402–408.
17. Zhu, Y.; Wang, L.; Hao, J.; Yin, P.; Zhang, J.; Li, Q.; Zhu, L.; Wei, Y. Palladium-catalyzed Heck reaction of polyoxometalate-functionalised aryl iodides and bromides with olefins. *Chem. Eur. J.* **2009**, *15*, 3076–3080.
18. Xu, B.; Peng, Z.; Wei, Y.; Powell, D.R. Polyoxometalates covalently bonded with terpyridine ligands. *Chem. Commun.* **2003**, *375*, 2562–2563.
19. Hirata, S.; Head-Gordon, M. Time-dependent density functional theory within the Tamm-Dancoff approximation. *Chem. Phys. Lett.* **1999**, *314*, 291–299.
20. Yanai, T.; Tew, D.P.; Handy, N.C. A new hybrid exchange-correlation functional using the Coulomb-attenuating method (CAM-B3LYP). *Chem. Phys. Lett.* **2004**, *393*, 51–57.
21. Weigend, F.; Ahlrichs, R. Balanced basis sets of split valence, triple zeta valence and quadruple zeta valence quality for H to Rn: Design and assessment of accuracy. *Phys. Chem. Chem. Phys.* **2005**, *7*, 3297–3305.
22. Tao, J.; Perdew, J.; Staroverov, V.; Scuseria, G. Climbing the Density Functional Ladder: Nonempirical Meta-Generalized Gradient Approximation Designed for Molecules and Solids. *Phys. Rev. Lett.* **2003**, *91*, 146401.
23. Grimme, S.; Antony, J.; Ehrlich, S.; Krieg, H. A consistent and accurate ab initio parametrization of density functional dispersion correction (DFT-D) for the 94 elements H-Pu. *J. Chem. Phys.* **2010**, *132*, 154104.
24. Grimme, S.; Ehrlich, S.; Goerigk, L. Effect of the damping function in dispersion corrected density functional theory. *J. Comput. Chem.* **2011**, *32*, 1456–1465.

25. Goerigk, L.; Grimme, S. Assessment of TD-DFT methods and of various spin scaled CIS(D) and CC2 versions for the treatment of low-lying valence excitations of large organic dyes. *J. Chem. Phys.* **2010**, *132*, 184103.
26. Janjua, M.R.S.A. Quantum mechanical design of efficient second-order nonlinear optical materials based on heteroaromatic imido-substituted hexamolybdates: First theoretical framework of POM-based heterocyclic aromatic rings. *Inorg. Chem.* **2012**, *51*, 11306–11314.
27. Melcamu, Y.Y.; Wen, S.; Yan, L.; Zhang, T.; Su, Z. Theoretical investigation of second-order nonlinear optical response by linking hexamolybdate with graphene in the donor-acceptor (D-A) framework. *Mol. Simul.* **2013**, *39*, 214–219.
28. Osakai, T.; Himeno, S.; Saito, A.; Hori, T. Electrochemical reduction of hexamolybdate(2−) ion in acidic aqueous-organic media. *J. Electroanal. Chem. Interfacial Electrochem.* **1990**, *285*, 209–221.
29. MarvinSketch. Available online: http://www.chemaxon.com (accessed on 27 April 2015).
30. Borg, S.J.; Best, S.P. Spectroelectrochemical cell for the study of interactions between redox-activated species and moderate pressures of gaseous substrates. *J. Electroanal. Chem.* **2002**, *535*, 57–64.
31. Lee, B.Y.; Kwon, H.Y.; Lee, S.Y.; Na, S.J.; Han, S.I.; Yun, H.; Lee, H.; Park, Y.W. Bimetallic anilido-aldimine zinc complexes for epoxide/CO_2 copolymerization. *J. Am. Chem. Soc.* **2005**, *127*, 3031–3037.
32. Furche, F.; Ahlrichs, R.; Hättig, C.; Klopper, W.; Sierka, M.; Weigend, F. Turbomole. *Wiley Interdiscip. Rev. Comput. Mol. Sci.* **2014**, *4*, 91–100.
33. Neese, F. The ORCA program system. *Wiley Interdiscip. Rev. Comput. Mol. Sci.* **2012**, *2*, 73–78.
34. Lin, Y.; Li, G.; Mao, S.; Chai, J. Long-Range Corrected Hybrid Density Functionals with Improved Dispersion Corrections. *J. Chem. Theory Comput.* **2013**, *9*, 263–272.